Impact of Satellite Transponder Nonlinearities on the Performance of Protected Tactical Waveform (PTW) for the Return Link (RL)

Lan K. Nguyen*, Richard B. Wells †, Khanh D. Pham‡
*LinQuest Corp, Los Angeles, CA
† Dept. of Electrical Engineering, University of Idaho, Moscow, ID
‡ Air Force Research Laboratory, Kirtland AFB, NM

Abstract — **This paper examines the impact of satellite transponder nonlinearities on the performance of protected tactical waveform (PTW) for the return link (RL). The performance impact due to adjacent channels interference (ACI) and a partial band noise jammer (PBNJ) are considered in the paper. In this paper, a Shaleh model is used to model the transponder traveling wave tube amplifier (TWTA). This TWTA is protected by a soft limiter to prevent TWTA operation in the saturation region. Impact of signal clipping due to this soft limiter under a PBNJ is also investigated. Computer simulations are performed using Digital Video Broadcasting – Satellite – Second generation (DVB-S2) forward error correcting (FEC) codes. In addition, a ground hub receiver does not assume knowledge of the channel information. Ground hub is required to estimate signal-to-noise ratio (SNR) and details of SNR estimation are also discussed in the paper.**

Keywords — ***Transponder; Nonlinearity; Multicarrier; Adjacent Channels Interference (ACI); Partial Band Noise Jammer (PBNJ); DVB-S2; Protected Tactical Waveform (PTW).***

I. INTRODUCTION

At the conclusion of a two-year study effort for protected MILSATCOM Design for Affordability Risk Reduction (DFARR) [1], Protected Tactical Waveform (PTW) [2] is adopted to support future wideband communication services. PTW is designed to provide protected communication services against various interference and jamming threats. To achieve this objective, PTW utilizes frequency diversity, time diversity, and powerful forward error correction (FEC) coding. Frequency diversity is achieved by frequency hopping spread spectrum (FHSS) technique; time diversity is achieved by time permutation, time division multiple access (TDMA) and interleavers; and FEC is performed by Digital Video Broadcasting – Satellite Second generation (DVB-S2) FEC [3]. This powerful FEC is based on the concatenation of BCH (Bose-Chaudhuri-Hocquengham) and LDPC (Low Density Parity Check) codes.

A traveling wave tube amplifier (TWTA) is a high gain, low noise, wide bandwidth microwave amplifier, its bandwidth is in the range of 300 MHz to 300 GHz [4]. It provides significant high power output and effiencies. It is capable of gains greater than 40 dB. For these reasons, TWTA is commonly used in satellite communication and is the primary amplification element of the transponder. It is also the largest contributor to transmission nonlinearities. TWTA causes both amplitude (AM-AM) and phase (AM-PM) distortions [5, 6, 7]. A multicarrier signal typical exhibits high peak-to-average power ratio (PAR). When this signal passes through a nonlinear TWTA, nonlinear distortions occur and intermodulation (IM) [5, 8] products are generated, which result in spectral regrowth. In nominal operation, input power backoff (IBO) is implemented so that the TWTA is operating in the linear region. In addition, the TWTA is often protected by another nonlinear device, a soft limiter which prevents the signal running into the saturation region, causing thermal instability which can damage the TWTA. For hopping signals, the transponder gain is typically assigned a priori. This gain is assigned based on user traffic, resource allocation: power, channel bandwidth, and time slots for each user so that the TWTA can be operating in the linear region. However, during operation, the link is often changed due to weather and interference power levels; the hub periodically measures the link signal-to-noise ratio (SNR) so that the transponder gain can be updated and adjusted accordingly.

There are two classes of interference 1) unintentional interference and 2) intentional jamming interference. Unintentional interference consists of adjacent channel interference (ACI), co-channel interference (CCI), and adjacent satellite interference (ASI). With power control and proper planning, unitentional interference can be managed as part of the allocation of the implementation loss budget. Intentional interference is caused by adversary jammers. Their goal is to interrupt, deny users' communication services or at least reduce users' throughput and data rates. A high power jammer can turn on and off its power at random. Its objective is to damage the hardware and to degrade the signal quality. In order to protect the TWTA, there are two potential solutions: 1) a soft limiter or 2) an automatic gain controller (AGC). A soft limiter is used to limit the magnitude of the signal if it exceeds a certain threshold while maintaining the phase information of the signal. An automatic gain controller has the ability to adjust the gain of the transponder on a hop-to-hop basis so that the signal is not clipped. A soft limiter is essenially another nonlinear device.

In this study, a Shaleh model [9, 10] is used for the TWTA. To simplify simulation and the analysis, a gain element, a soft limiter and a TWTA are used to model the transponder. Computer simulations are used to evaluate the performance impacts due to ACI and PBNJ on the return link (RL). A notional block diagram of a single beam for the RL is shown in Fig. 1. Under PBNJ, impacts of the transponder nonlinearities caused by a soft limiter will be evaluated and compared against an automatic gain controller. In addition, the ground hub receiver does not assume knowledege of the channel. The

978-1-5090-3781-0/16/$31.00 ©2016 IEEE

ground hub receiver is required to estimate the SNR for its DVB-S2 decoder.

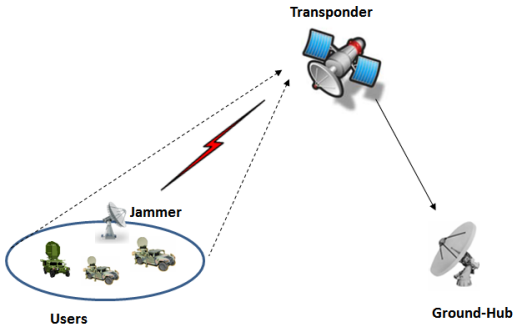

Fig. 1. Notional return link (RL) block diagram.

II. System Model

The end-to-end top level simulation block diagram for the RL is shown in Fig. 2. At the input, packets of 1500 bytes are sent to the DVB-S2 encoder. The M-ary Phase Shift Keying (MPSK) modulator takes the coded bits and then maps them to form Gray-coded MPSK symbols. The MPSK modulated symbols enter the channel interleaver and are grouped into equal length sequences which form the hops. Reference symbols are then added to each hop. Each hop is then transmitted at a different frequency. Reference symbols and the distribution of reference symbols are known a priori at the ground hub receiver; data symbols contain the information bits. This process is identical for ACI channels. At the input of the transponder, the aggregated input signal includes signal of interest (SOI), ACI signals, uplink (UL) noise, and an adversary jammer. The transponder relays the signal on the downlink (DL). The performance impact due to transponder nonlinearities and noise power robbing are exhibited on the downlink. At the ground hub receiver, known reference symbols are demultiplexed to estimate phase/frequency errors and channel SNR. Received signal is de-interleaved, demodulated, and decoded by the DVB-S2 decoder. Decoded packets are then compared with transmitted packets to determine packet error rate (PER).

In the discrete time domain, at the input of the transponder the signal is given by

$$y(k) = s_i(k) + \sum_{m=1}^{N} s_{aci}(k,m) + v_k \cdot n_j(k) + n_{ul}(k) \quad (1)$$

where $s_i(\cdot)$ denotes SOI, $s_{aci}(\cdot)$ denotes ACI signal, $v_k \in \{0,1\}$ is a random variable, $v_k = 1$ with probability hit ρ. Otherwise, $v_k = 0$, $n_j(\cdot)$ denotes the jamming signal, and $n_{ul}(\cdot)$ denotes UL channel noise, complex-value, additive white Gaussian noise (AWGN), with two-sided power spectrum density N_o.

Signal of interest is given by

$$\begin{aligned} s_i(k) &= s_i(kT_s) \\ &= a_k \textstyle\sum_n d_n g\left(kT_s - nT_{sym,soi}\right) \cdot e^{j\varphi_{err}(kT_s)} \end{aligned} \quad (2)$$

where k denotes the sample index, a_k denotes signal amplitude, $\{d_n\}$ denotes transmitted symbols from the MPSK alphabet, T_s denotes the sample period which is normalized to 1, $T_{sym,soi}$ denotes the symbol period of the signal of interest, $g(\cdot)$ denotes the spectral shaping filter, and $\varphi_{err}(\cdot)$ denotes the total phase error. The spectral shaping filter is chosen to satisfy the Nyquist zero intersymbol interference (ISI) criterion. A raised cosine (RC) filter is considered in the paper. The transmitter and receiver filters are jointly designed for zero ISI. Therefore, the spectral shaping filter is a square root raised cosine (SRRC) filter.

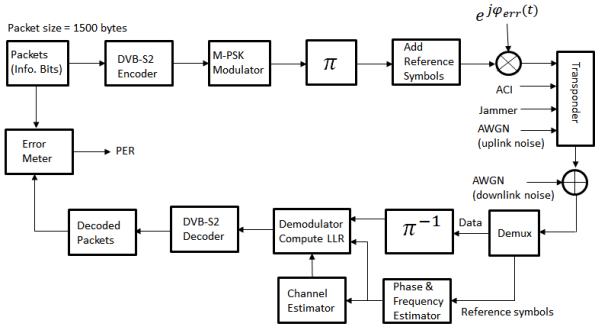

Fig. 2. Return link (RL) end-to-end block diagram.

The frequency response of the SRRC filter is given by

$$G(f) = H_{SRRC}(f) \quad (3)$$

and

$$H_{SRRC}(f) = \sqrt{H_{RC}(f)}, \quad (4)$$

where the frequency response of an ideal RC filter is [11]

$$H_{RC}(f) = \begin{cases} T_{sym}, & 0 \le |f| \le \frac{1-\beta}{2T_{sym}} \\ \frac{T_{sym}}{2}\left[1 + \cos\left(\frac{\pi T_{sym}}{\beta}\left(|f| - \frac{1-\beta}{2T_{sym}}\right)\right)\right], & \frac{1-\beta}{2T_{sym}} \le |f| \le \frac{1+\beta}{2T_{sym}} \\ 0, & |f| > \frac{1+\beta}{2T_{sym}} \end{cases} \quad (5)$$

and $\beta = 0.2$ is the roll-off factor. The impulse response of a SRRC filter with $\beta = 0.2$, truncated after $\pm 7T_{sym}$ is shown in Fig. 3. The total phase error is a function of unknown phase error and frequency error. It is given by

$$\varphi_{err}(k) = \varphi_0 + 2\pi \cdot f_{err}(k) \cdot k \cdot T_s, \quad (6)$$

$$\varphi_0 \sim U[-\pi, \pi). \quad (7)$$

In this paper, frequency error is assumed to be small, for simulation convenience, the integrated phase error caused by it by the end of a hop period equals $\pi/4$.

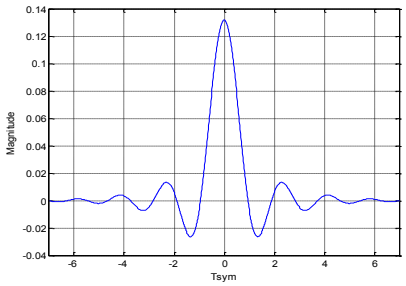

Fig.3. SRRC impulse response, roll-off factor $\beta = 0.2$.

The channel spacing between two signals is given by

$$\Delta f_i = 1.33 \left(\frac{R_i + R_{i+1}}{2}\right) \tag{8}$$

where R_i and R_{i+1} denote the symbol rates of the i[th] and (i+1)[th] users, respectively. The symbol rate of the i[th] user is given by

$$R_i = \frac{1}{T_{sym,i}}. \tag{9}$$

A. Transponder Model

In this paper, the transponder consists of a gain element, a soft limiter and a TWTA. Transponder gain can either be fixed or adjustable (automatic gain control.) This gain is used to ensure the TWTA operates in the linear region. The performance impact due to transponder gain is discussed in Section III of the paper. The block diagram of the transponder is shown in Fig. 4.

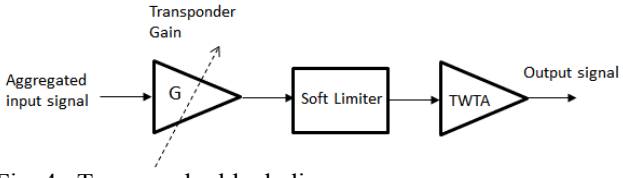

Fig. 4. Transponder block diagram.

The primary purpose of a soft limiter is to prevent the signal running into the saturation region of the TWTA. The instantaneous nonlinear characteristics of the soft limiter is given as

$$S_L(x) = \begin{cases} x, & |x| \le R \\ Re^{iarg(x)}, & |x| > R \end{cases}. \tag{10}$$

A Shaleh model for nonlinear amplitude and phase distortions is assumed for the TWTA. The two-parameter formulas that represent the amplitude and phase distortions are given by

$$A(r) = \frac{\alpha_a r}{1+\beta_a r^2} \quad (AM-AM) \quad \text{(Normalized)} \tag{11}$$

$$\Phi(r) = \frac{\alpha_\varphi r^2}{1+\beta_\varphi r^2} \quad (AM-PM) \quad \text{(Rad)} \tag{12}$$

where

$$\alpha_a = 2,\ \beta_a = 1,\ \alpha_\varphi = 4,\ \beta_\varphi = 9.1, \quad [9, 10] \tag{13}$$

and r denotes the instantaneous magnitude of the signal. To simplify the analysis, the above AM-AM distortion parameters are chosen so that the peak is normalized at unity. The magnitude and phase characteristics of the TWTA are shown in Fig. 5.

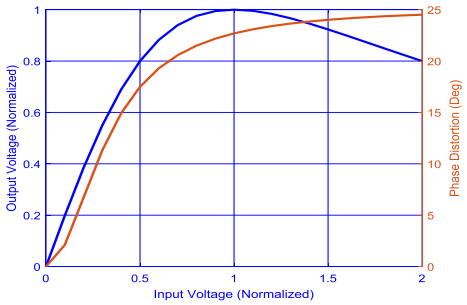

Fig. 5. TWTA AM-AM and AM-PM characteristics.

The output signal of the TWTA consists of 2 components, an undistorted component and a distorted component. The distorted component is due to intermodulation (IM) products. The average output power is given by

$$P_o = P_s + P_{IM} \tag{14}$$

where P_s denotes the desired or undistorted output signal power and P_{IM} denotes the distortion power, the average IM noise power.

At the input of the TWTA, the magnitude of $r(t)$ follows Rayleigh statistics. The Rayleigh distribution is given by

$$f(r;\sigma_r) = \frac{re^{\frac{-r^2}{2\sigma_r^2}}}{\sigma_r^2}, \quad r \ge 0 \tag{15}$$

where σ_r denotes the scale parameter of the Rayleigh distribution. Using Bussgang's theorem [12] and the Rayleigh statistics of the signal magnitude, undistorted signal power can be computed, and it is given by

$$P_s = \frac{4}{P_{in}} + \frac{8}{P_{in}^2} e^{\frac{1}{P_{in}}} Ei\left(\frac{-1}{P_{in}}\right) + \frac{4}{P_{in}^3} e^{\frac{2}{P_{in}}} Ei^2\left(\frac{-1}{P_{in}}\right) \tag{16}$$

where

$$\mathrm{Ei}(x) = \int_{-\infty}^{x} \frac{e^t}{t} dt \tag{17}$$

and

$$P_{in} = 2\sigma_r^2 \tag{18}$$

where P_{in} denotes the input power to the TWTA. In this study, the TWTA nominally operates in the linear region and an IBO value of 7 dB is used, i.e.

$$P_{in} = 10^{-IBO} = 10^{-0.7} = 0.1995. \tag{19}$$

Using (11) and (16), AM/AM and undistorted output power curves are shown in Fig. 6.

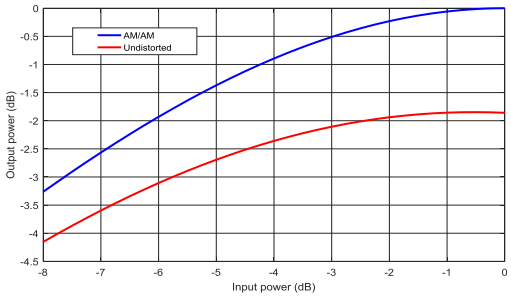

Fig. 6. Shaleh Model AM/AM and undistorted power P_s

In addition, for the Rayleigh distribution, the expected clipping power by a soft limiter as a function of clipping threshold R is given by

$$P_{clip} = \int_R^{\infty} (r - R)^2 \, f(r; \sigma_r) dr. \tag{20}$$

Substituting (15) into (20) and evaluating the integral one obtains

$$P_{clip} = \; 2\sigma_r^2 e^{-\frac{R^2}{2\sigma_r^2}} - \sqrt{\frac{\pi}{2}} \sigma_r R \; erfc\left(\frac{R}{\sigma_r}\sqrt{\frac{1}{2}}\right) \tag{21}$$

where

$$erfc(x) = \frac{2}{\pi}\int_x^{\infty} e^{-t^2} dt. \tag{22}$$

Substituting (18) and (19) into (21), the expected clipping power as a function of threshold R normalized to signal magnitude standard deviation is shown in Fig. 7. Results shown in Fig. 7 indicate that for the threshold value at $2\sigma_r$, the input power threshold $P_{in}^R = 2P_{in} = 0.399$, which corresponds to $IBO =$ 4 dB, the expected clipping power is about 1.8 % and 3.4% relative to the total TWTA output power P_o and undistorted power P_s, respectively. On the other hand, if the limiter threshold is at $3.2\sigma_r$, the TWTA is at saturation and the expected clipping power is negligible.

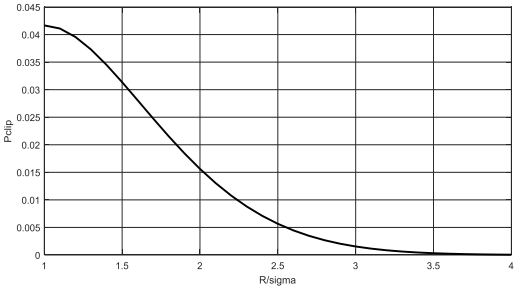

Fig. 7. P_{clip} vs. R/σ_r for IBO = 7 dB.

B. Partial Band Noise Jammer (PBNJ) Model

A PBNJ [13, 14] spreads its power over ρ $(0 < \rho \leq 1)$ fraction of the hopping bandwidth. Also, ρ represents the probability of a hop being jammed. Under PBNJ, the signal over total noise and interference is given by

$$SINR = \frac{P_r}{N_o + \frac{J_o}{\rho} + IM_o} = \frac{P_r}{N_o\left[1 + \frac{1}{N_o}\left(\frac{J_o}{\rho} + IM_o\right)\right]}, \tag{23}$$

$$J_o = \frac{J}{W_T} \quad \text{and} \quad IM_o = \frac{P_{IM}}{W_T} \tag{24}$$

where P_r denotes SOI power, J denotes jammer power, J_o denotes full-band (FB) $(\rho = 1)$ noise density level, N_o denotes UL noise density, IM_o denotes IM density level, and W_T denotes the hopping bandwidth.

For a transponder which does not employ an AGC, i.e. a transponder uses a soft limiter, as a PBNJ power enters the TWTA, the nominal operating point is pushed up toward the saturation region which results in higher IM power as shown in Fig. 6.

In dB, the additional SNR required to compensate a FB jammer is given by

$$\Delta SNR_{inc} = 10log_{10}\left(1 + \frac{J_o + IM_o}{N_o}\right). \tag{25}$$

Note: Since all the signals are sharing the transponder, in addition to IM products, the signal power is robbed by the jammer power. Interested readers are referred to [15] for more details. Impacts of IM products and power sharing are discussed in Section III of the paper.

C. Phase and Frequency Error Estimate

In this paper, known reference symbols are used to estimate phase and frequency errors [16]. Reference symbols are assumed to be at both ends of the hop. Average phase rotation at each end of the hop is given by

$$\phi_k = \frac{1}{N_{R_k}} arg\left\{\sum_{n=1}^{N_{R_k}} y_k(n) r_k^*(n)\right\}, \quad k = 1, 2 \tag{26}$$

where subscript k denotes the front and back sets of data symbols, $y_k(\cdot)$ denotes receiving reference symbols, $r_k(\cdot)$ denotes known reference symbols, N_{R_1} and N_{R_2} denote the numbers of reference symbols at the front and back of the hop, respectively, and * denotes complex conjugate operation. The total number of reference symbols in a hop is given by

$$N_R = N_{R_1} + N_{R_2}. \tag{27}$$

The amount of phase shift between the front and back groups of reference symbols is given by

$$\Delta\Phi = \phi_2 - \phi_1. \quad (28)$$

$\Delta\Phi$ is spread linearly over N data symbols plus $N_R/2$ reference symbols, where N denotes number of data symbols in a hop. Using (28), each data symbol can be phase adjusted accordingly. For small numbers of reference symbols, techniques described in [17] can be applied.

D. Channel SNR Estimate

SNR is an important parameter for the computation of the log-likelihood ratio (LLR), which is used in the DVB-S2 decoder. SNR estimation consists of two stages. The first stage is the per hop SNR estimation. This stage is aided by reference symbols. It is given by [18]

$$SNR(i) = \frac{\left[\frac{1}{N_R}\sum_{n=0}^{N_R-1} Re\{y(n)^* r(n)\}\right]^2}{\frac{1}{N_R-1.5}\sum_{n=0}^{N_R-1}|y(n)|^2 - \frac{1}{N_R(N_R-1.5)}\left[\sum_{n=0}^{N_R-1} Re\{y(n)^* r(n)\}\right]^2}. \quad (29)$$

The second stage is the per code word SNR estimation. It is given by

$$SNR_w = Median[SNR(i)],\ i = 1,2,\cdots N_h \quad (30)$$

where N_h denotes number of hops per code word. In this stage, the median operation is used to remove biases, outliers, and artifacts obtained in stage 1 due to low SNR and residual phase and frequency errors. Long term SNR estimates that incorporate channel condition, i.e., rain rate will be reported in future work.

III. SIMULATION RESULTS

Computer simulations for Quadrature Phase Shift Keying (QPSK) with code rates of 1/2 and 1/3 are considered. The simulations are performed using packet size of 1500 bytes with a target PER of 10^{-3}. Performance of the DVB-S2 decoder under AWGN with phase and frequency errors recovery is shown in Fig. 8.

For PER of 10^{-3}, as expected, the results shown in Fig. 8 indicate that that there is a tradeoff between power and data rates. The data rate for QPSK 1/3 is lower than QPSK 1/2. However, QPSK 1/3 requires 1.5 dB less power.

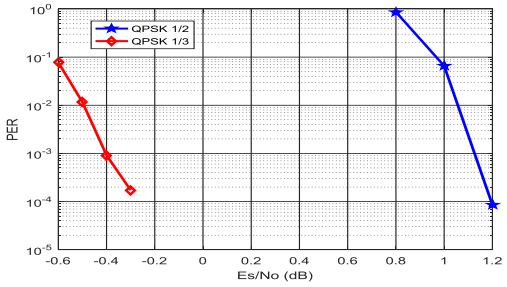

Fig. 8. PER for QPSK with code rates 1/2 and 1/3.

A. ACI Performance

Consider a 5-user scenario. The SOI is in the middle of the channel group, occupies the smallest bandwidth, and communicates with the lowest data rate. The signal power spectrum is shown in Fig. 9.

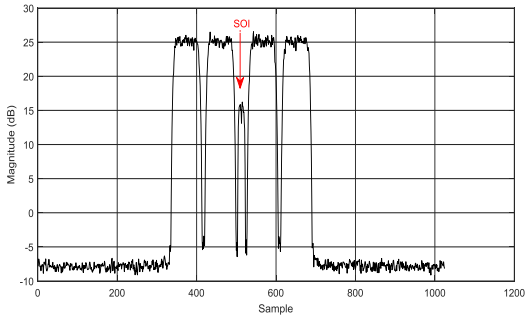

Fig. 9. Users' power spectrum, ACI scenario.

As shown in Fig. 9. The SOI is placed next to very high power users. ACI is due to unwanted power spill over to the SOI channel. The amount of degradation as a function of the power spectrum densities of ACI relative to SOI is shown in Fig. 10.

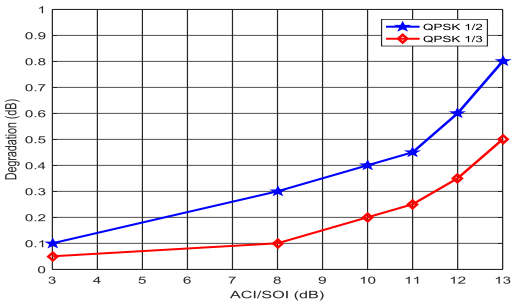

Fig. 10. ACI degradation for QPSK code rates 1/2 and 1/3.

Note: The amount of ACI shown in Fig. 10 includes both left and right adjacent users. Results shown in Fig. 10 indicate that code rate 1/3 is more robust than code rate 1/2. For ACI/SOI of 13 dB, performance degradations of 0.8 dB and 0.5 dB are expected for code rate 1/2 and code rate 1/3, respectively.

B. PBNJ Performance

The PBNJ performance for QPSK code rate 1/3, $J_o/N_o = 10$ dB, with AGC and with soft limiter $R = 2\,\sigma_r$ and $R = 3.2\,\sigma_r$ is shown in Fig. 11. Results shown in Fig. 11 indicate

- For full-band jamming, $\rho = 1$, the expected SNR should be 10 dB. However, the required SNR is higher than 10 dB. Ground hub requires an additional of 0.4 dB and 0.7 dB when the transponder uses AGC and with a soft limiter, respectively. These additional power requirements are due to IM products and power sharing, jammer power robbing, of the transponder.

- With a soft limiter, there is no performance advantage for setting a large threshold of $R = 3.2\,\sigma_r$ versus $R = 2\,\sigma_r$.
- Relative to full-band jamming, there is a PBNJ advantage of 2.8 dB and 1.2 dB at $\rho = 0.1$ for transponder with soft limiter and AGC, respectively.

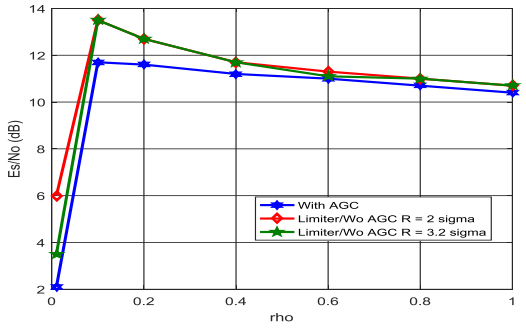

Fig. 11. PBNJ performance for QPSK 1/3, $J_o/N_o = 10$ dB, with AGC and limiter $R = 2\,\sigma_r$ and $3.2\sigma_r$.

IV. Conclusion

We use a simple transponder model which includes a gain element, a soft limiter, and a Shaleh model for the TWTA. Using this simple transponder model, the impact of the transponder nonlinearities due to a soft limiter and a TWTA to the PTW waveforms on the RL is characterized. During nominal operation, the TWTA is required to operate in the linear region and the transponder gain is calibrated to serve that purpose. Transponder gain can either be fixed or adjusted on a hop-to-hop basis. With the AGC, the TWTA is guaranteed to operate at the desired operating point regardless of the input power. Without the AGC, the transponder relies on a soft limiter to ensure the signal does not run into the saturation region. In this case, the gain is fixed and precomputed during the planning stage. At the nominal operating point, depending upon the threshold limit, the expected clipping power by the soft limiter can also be characterized. QPSK with code rates 1/2 and 1/3 are considered in this study. A ground receiver uses reference symbols to estimate phase/frequency errors and channel SNR. SNR estimates consists of two stages, per hop and per code word estimates. Under ACI environment, with ACI/SOI of 13 dB, degradations of 0.8 dB and 0.5 dB are recorded for code rates 1/2 and 1/3, respectively. Degradation due to PBNJ is also investigated for the transponder with an AGC and with a soft limiter. For a soft limiter, relative to nominal operating point, under PBNJ with $J_o/N_o = 10$ dB, there is no performance advantage of setting large threshold limit at saturation of $3.2\,\sigma_r$ versus $2\,\sigma_r$. We showed that the impact due to a soft limiter is more severe than the AGC. Under full band jamming, due to IM products and power sharing, we showed that signal requires additional 0.4 dB and 0.7 dB for AGC and soft limiter, respectively. In addition, relative to full band jamming, there is a PBNJ performance advantage of 1.2 dB and 2.8 dB for AGC and soft limiter, respectively. In all cases, we showed that if the transponder employs an AGC then the degradation can be minimized.

Acknowledgment

The authors would like to thank the reviewers for all the comments.

References

[1] Sullivan, J.; Glaser, M.; Walsh, C.; Dallas, W.; Blackman, J., VanderVennet, J; Shunshine, C.; Chuang, J. C., "Protected Tactical MILSATCOM Design for Affordability Risk Reduction (DFARR) Results," IEEE MILCOM Proceedings, 2014.

[2] Wolf, B. J.; Huang, J. C., "Implementation and Testing of the Protected Tactical Waveform (PTW)," IEEE MILCOM Proceedings, 2015.

[3] ETSI EN 302 307 v1.2.1 (2009-08): Digital Video Broadcasting (DVB), Second generation framing structure, channel coding and modulation systems for Broadcasting, Interative Services, News gathering and other broadband satellite applications (DVB-S2).

[4] Industrial Assessment of the Microwave Power Tube Industry, Department of Defense, USA, April 1997.

[5] Shimbo, O., "Effects of Intermodulation, AM-PM Conversion, and Additive Noise in Multicarrier TWT Systems," Proc. IEEE, vol. 59, pp. 230-238, Feb. 1971.

[6] Rowe, H. E. "Memoryless Nonlinearities with Gaussian Inputs: Elementary Results," Bell Syst. Tech Journal, vol. 61, no. 7, pp 1520–1523, Sep. 1982.

[7] Minkoff, J., "The Role of AM-to-PM Conversion in Memoryless Nonlinear Systems," IEEE Trans on comm., vol. COM-33, no. 2, pp 139-144, Feb. 1985.

[8] Sunde, E. D., "Intermodulation Distortion in Multicarrier FM Systems," IEEE International Convention, pp. 130-146, Mar. 1965.

[9] Shaleh, A. A. M, "Frequency-Independent and Frequency-Dependent Nonlinear Model of TWT Amplifiers," IEEE Trans on comm., vol. 29, pp 1715-1720, 1981.

[10] Qureshi, M. E.; Wilson, S. E., "Particle Filter Based Inversion of Nonlinear Satcom Channels," IEEE MILCOM Proceedings, pp 604-609, 2014.

[11] Proakis, J. G., *Digital Communications*, 4th Edition, Mc Graw Hill, New York, NY, 2001.

[12] Bussgang, J. J., "Crosscorrelation Functions of Amplitude-Distorted Gaussian Signals," Research Lab. Electron, M.I.T. Tech Report No. 216, 1952.

[13] Yao, H.; Huang, J. C.; Wornell, G. W., "Achieving High Bandwidth Efficiency Under Partial-Band Noise Jamming," IEEE MILCOM Proceedings, 2013.

[14] Nguyen, L. K.; Truong, T. V., "On the Performance of Serially Concatenated Convolutional Code for Frequency Hopped PSK in Partial-Band Noise Jammer," IEEE MILCOM Proceedings, 2009.

[15] Nguyen, L. K.; Wells, R. B; Le-ngoc, T., "Power Allocation for Shared and Frequency Hopped Transponder," IEEE MILCOM Proceedings, 2015.

[16] Fechtel, S. A.; "OFDM Carrier and Sampling Frequency Synchronization and its Performance on Stationary and Mobile Channels," IEEE Trans. Comm. pp. 438-441, Aug. 2000

[17] Nguyen, L. K.; Wells, R. B., "Doppler Shift Cancellation Using Phasor and Split Phasor LMS Algorithms," IEEE MILCOM Proceedings, 2008.

[18] Pauluzzi, D. R.; Beaulieu N. C., "A Comparison of SNR Estimation Techniques for the AWGN Channel," IEEE Trans Comm. pp. 1681-1691, Oct. 2000.